

# Structure of Cathodically Deposited Nickel Hexacyanoferrate Thin Films Using XRD and EXAFS

William A. Steen,<sup>†</sup> Sang-Wook Han,<sup>‡</sup> Qiuming Yu,<sup>‡</sup> Robert A. Gordon,<sup>§</sup>  
Julie Olmsted Cross,<sup>§</sup> Edward A. Stern,<sup>‡</sup> Gerald T. Seidler,<sup>‡</sup>  
Kavita M. Jeerage,<sup>†</sup> and Daniel T. Schwartz<sup>\*,†</sup>

Departments of Chemical Engineering & Physics, University of Washington, Seattle, Washington 98195, and Pacific Northwest Consortium Collaborative Access Team (PNC-CAT), Advanced Photon Source, Argonne National Laboratory, Argonne, Illinois 60439

Received April 15, 2002. In Final Form: June 24, 2002

X-ray diffraction (XRD) and extended X-ray absorption fine structure (EXAFS) data were used to explore the structure of cathodically deposited thin films of nickel hexacyanoferrate (NiHCF). Thin films were electrodeposited on Pt substrates and analyzed in both the reduced and oxidized states and when intercalated with Cs<sup>+</sup>, K<sup>+</sup>, and mixtures of Cs<sup>+</sup>/K<sup>+</sup>. All experiments were performed at room temperature. XRD data provided lattice parameters and confirmed the cubic nature of this polycrystalline material, but it could not establish the exact space group from the many known to exist for this class of materials. The lattice parameter monotonically increased from ca. 10.15 to 10.21 Å as the fraction of intercalated cation went from 100% K<sup>+</sup> to 100% Cs<sup>+</sup>. EXAFS data permitted the determination of average nickel coordination, a property directly related to the material's refined structure. Fe and Ni K-edge data were fit using feffit2.32 and FEFF7; the data were fit simultaneously in order to break the correlation between coordination number and the Debye–Waller factor. This resulted in mean nickel coordination values between 4.4 and 5.1 and estimated lattice parameters which are ca. 0.1 Å greater than those found from XRD, a trend indicative of local disorder within the sample.

## Introduction

Electrochemically switched ion exchange (ESIX) processes use the selectivity of an ion intercalation compound to perform a separation.<sup>1–3</sup> To separate a dilute target ion and concentrate it using ESIX requires a material with a high affinity for the target ion, a large ion intercalation capacity, and the ability to deintercalate most of the intercalated ions via electrochemical modulation of the matrix charge density.<sup>4</sup> Nickel hexacyanoferrate (NiHCF), a polynuclear coordination compound in the Prussian Blue family,<sup>5</sup> is a candidate for separations involving alkali cations.<sup>1,2</sup>

NiHCF can be made as an electroactive thin film by anodic derivatization of a nickel substrate in the presence of ferricyanide anions<sup>6,7</sup> or by cathodic deposition onto a conductive substrate in a solution containing divalent nickel and ferricyanide anions.<sup>8</sup> Both cathodically deposited and anodically derivatized films display excellent

selectivity for Cs<sup>+</sup> in the presence of other alkali cations.<sup>1,2,9</sup> Cathodically deposited thin films are the focus of our work because they tend to have larger ion exchange capacities than derivatized films.

To function as an ideal ESIX material, NiHCF must be able to deintercalate a large fraction of the intercalated alkali cations. The efficiency of this deintercalation process is intimately tied to the stoichiometry and structure of the thin film. Energy-dispersive X-ray spectroscopy (EDS) results show that cathodically deposited films are only able to deintercalate approximately 75% of their alkali cations upon oxidation of the matrix,<sup>10</sup> implying a redox reaction and stoichiometry roughly analogous to



Here, A denotes an intercalated alkali cation and A<sup>+</sup> denotes an alkali cation deintercalated into solution.

Though the intercalation stoichiometry of eq 1 has been established for cathodically deposited NiHCF,<sup>10</sup> the actual structure of the thin film has not been analyzed. The literature of bulk metal hexacyanoferrates suggests that stoichiometry is closely linked to structure.<sup>11,12</sup> Specifically, the structure normally associated with eq 1 consists of Fe(CN)<sub>6</sub> vacancies from an otherwise perfect network of 6-fold coordinated Fe–C≡N–Ni chains. Figure 1a shows the oxidized form of this structure (space group: *Pm-3m*), which is a structural analogue of “insoluble” Prussian Blue. This unit cell has three square-planar and one octahedrally coordinated nickel atoms resulting in an average Ni

<sup>†</sup> Department of Chemical Engineering, University of Washington.

<sup>‡</sup> Department of Physics, University of Washington.

<sup>§</sup> Argonne National Laboratory.

\* To whom correspondence should be addressed.

(1) Lilga, M. A.; Orth, R. J.; Sukamto, J. P. H.; Haight, S. M.; Schwartz, D. T. *Sep. Purif. Technol.* **1997**, *11*, 147–158.

(2) Rassat, S. D.; Sukamto, J. H.; Orth, R. J.; Lilga, M. A.; Hallen, R. T. *Sep. Purif. Technol.* **1999**, *15*, 207–222.

(3) Bridger, N. J.; Jones, C. P.; Neville, M. D. *J. Chem. Technol. Biotechnol.* **1991**, *50*, 469–481.

(4) Jeerage, K. M. *Characterization of Electrodeposited Nickel Hexacyanoferrate for Electrochemically Switched Ion Exchange*; University of Washington: Seattle, WA, 2001.

(5) Itaya, K.; Uchida, I.; Neff, V. D. *Acc. Chem. Res.* **1986**, *19*, 162–168.

(6) Sinha, S.; Humphrey, B. D.; Bocarsly, A. B. *Inorg. Chem.* **1984**, *23*, 203–212.

(7) Bocarsly, A. B.; Sinha, S. *J. Electroanal. Chem.* **1982**, *137*, 157–162.

(8) Bacskai, J.; Martinusz, K.; Czironk, E.; Inzelt, G.; Kulesza, P. J.; Malik, M. A. *J. Electroanal. Chem.* **1995**, *385*, 241–248.

(9) Jeerage, K. M.; Schwartz, D. T. *Sep. Purif. Technol.* **2000**, *35*, 2375–2392.

(10) Jeerage, K. M.; Steen, W. A.; Schwartz, D. T. *Chem. Mater.* **2002**, *14*, 530–535.

(11) Loos-Neskovics, C.; Fedoroff, M.; Garnier, E.; Gravelleau, P. *Talanta* **1984**, *31*, 1133–1147.

(12) Loos-Neskovics, C.; Fedoroff, M.; Garnier, E. *Talanta* **1989**, *36*, 749–759.

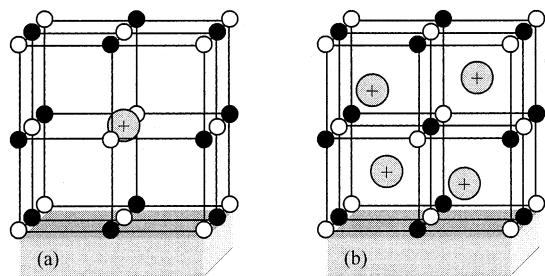


**Figure 1.** The structure on the left is electrodeposited NiHCF in the oxidized state (a), analogous to "insoluble" Prussian Blue (space group:  $Pm\bar{3}m$ ). The structure on the right (b) is analogous to "soluble" Prussian Blue, also in the oxidized state (space group:  $F\bar{4}3m$ ).  $\bullet$  is Fe,  $\circ$  is Ni,  $-$  is CN, and  $\oplus$  is an intercalated alkali cation.

coordination of 4.5. All of the Fe atoms are octahedrally coordinated. Of course, the same average stoichiometry can arise from different structures or mixtures of different metal hexacyanoferrate phases; both possibilities are well documented in the bulk NiHCF literature.<sup>11–13</sup>

NiHCF films prepared by anodic derivatization of a nickel substrate have, in general, been studied more than cathodically deposited materials. Prior studies of derivatized films normally start with the assumption that electroactive NiHCF is a structural analogue of "soluble" Prussian Blue (shown in Figure 1b in the oxidized state, space group  $F\bar{4}3m$ ), though very few studies have directly tackled the issue of thin film crystallinity and structure for electrochemically prepared materials.<sup>14–20</sup> Kelly et al. performed X-ray diffraction (XRD) studies on anodic thin film materials, confirming that these materials were crystalline with a cubic unit cell dimension comparable to bulk powders.<sup>17</sup> Because of the small quantities of material made, only low index planes were identifiable. These low index planes are mostly conserved among the various forms of NiHCF, including the structures shown in Figure 1a,b.<sup>21,22</sup> Given the diversity of stoichiometries and structures seen in bulk NiHCF powders as well as their known sensitivity to preparation procedures,<sup>11,12</sup> it is necessary to evaluate the thin film structure for various deposition schemes.

In this paper, we utilize XRD and extended X-ray absorption fine structure (EXAFS) to probe the crystallinity of cathodically grown NiHCF and the local environment of Fe and Ni in the structure. We explore the role of the intercalating cation on the structural traits of the solid by performing ion intercalation/deintercalation studies with  $\text{Cs}^+$ ,  $\text{K}^+$ , and mixtures of the two. These studies show that established relationships between stoichiometry and structure in bulk NiHCF, namely, that the stoichiometry is governed by  $\text{Fe}(\text{CN})_6$  vacancies from

the lattice, remain consistent with data for cathodically deposited thin films.

## Experimental Section

**Electrochemical.** Electrochemical experiments were performed using an EG&G PAR 263A potentiostat controlled with custom written LabView software. Platinum electrodes of 1 cm diameter and 1 mm thickness were prepared for electrochemistry by mirror polishing one face ( $0.785 \text{ cm}^2$ ). For all electrochemical experiments, only this polished surface was allowed to contact the electrolytes. The electrode was cleaned electrochemically in 1 M  $\text{H}_2\text{SO}_4$  by cyclic voltammetry (CV) from  $-275$  to  $1675 \text{ mV}$  vs a saturated calomel reference electrode (SCE) at  $100 \text{ mV/s}$ . Films of NiHCF were then deposited onto the polished face of the disk by cycling the potential from  $850$  to  $0 \text{ mV}$  vs SCE at  $25 \text{ mV/s}$  in a freshly mixed solution of  $0.002 \text{ M NiSO}_4$ ,  $0.002 \text{ M K}_3\text{Fe}(\text{CN})_6$ , and  $0.25 \text{ M Na}_2\text{SO}_4$ . This procedure was repeated for multiple substrates, resulting in NiHCF films with reversible charge densities (capacities) between  $10$  and  $15 \text{ mC/cm}^2$ , corresponding to a film thickness of a few hundred nanometers.

Four films were then soaked overnight in  $1 \text{ M CsNO}_3$ . (This was deemed necessary based on preliminary energy-dispersive X-ray results that showed residual amounts of  $\text{Na}^+$  and  $\text{K}^+$  left in the structure from electrodeposition.) Those films were then cycled  $50$  times at  $25 \text{ mV/s}$  from  $25$  to  $1125 \text{ mV}$  vs SCE in  $1 \text{ M CsNO}_3$ . Four additional films were cycled in  $1 \text{ M KNO}_3$  in the same manner. Finally, three films were cycled in  $1 \text{ M}$  solutions of varying amounts of  $\text{Cs}^+$  and  $\text{K}^+$  solutions. The solution mixtures were as follows:  $0.5 \text{ M CsNO}_3/0.5 \text{ M KNO}_3$ ,  $0.001 \text{ M CsNO}_3/0.999 \text{ M KNO}_3$ , and  $0.0001 \text{ M CsNO}_3/0.9999 \text{ M KNO}_3$ . These films were cycled in the same manner as the others (i.e.,  $50$  times from  $25$  to  $1125 \text{ mV}$  vs SCE at  $25 \text{ mV/s}$ ).

The films were then placed in either a reduced or oxidized state. Each film cycled in a mixed electrolyte, two of the films cycled in  $1 \text{ M KNO}_3$ , and two of the films cycled in  $1 \text{ M CsNO}_3$  were all held at the most reducing potential ( $25 \text{ mV}$ ) for  $15 \text{ min}$  and removed from solution while still under potential control. The remaining films were ramped (at  $25 \text{ mV/s}$ ) to their most oxidizing potential and then held there for  $15 \text{ min}$ . These films were removed from solution while still under potential control. Raman spectroscopy was used to confirm the oxidation state of the films.<sup>23</sup>

**X-ray Diffraction (XRD).** X-ray diffraction data were acquired on all of the films cycled in mixed electrolytes (three samples) and films cycled in both  $1 \text{ M CsNO}_3$  and  $1 \text{ M KNO}_3$  in both the reduced and oxidized state (four samples). XRD data were acquired at the Pacific Northwest Consortium Collaborative Access Team (PNC-CAT) bending magnet beamline (Sector 20) at the Advanced Photon Source (APS). Glancing angle ( $3^\circ$ ) experiments were performed at room temperature on spinning samples (spinning averages the response). Slit widths were set so that a footprint of approximately  $0.15 \text{ cm}^2$  was left on each sample (ca.  $20\%$  of sample). The incident excitation energy was  $8000 \text{ eV}$  ( $\lambda = 1.55 \text{ \AA}$ ). A four-circle kappa diffractometer was stepped in  $0.02^\circ$  increments, with an integration time of  $10 \text{ s}$  per point. An Oxford scintillation detector was swept from a  $2\Theta$  of  $10^\circ$  to  $80^\circ$ . Helium-filled tubes were used along the incident beam to decrease absorption of the X-rays. The monochromator was detuned to  $\sim 75\%$  maximum intensity to decrease harmonics.

**Powder X-ray Diffraction Simulations.** All simulated X-ray diffraction patterns were performed using the Diffraction-Crystal module in the materials simulation software package, Cerius<sup>2</sup> version 4.2 (MatSci, Molecular Simulations Inc., San Diego, CA, 2000). The wavelength was set to  $1.55 \text{ \AA}$ , and all other parameters were the default values. All crystal structures used for XRD pattern simulation were adopted from the final configurations after the molecular dynamics simulations of Yu et al.<sup>24</sup>

**Energy Dispersive X-ray Spectroscopy (EDS).** A scanning electron microscope (JEOL JSM-5200) operated at an accelerating voltage of  $15 \text{ keV}$  was used to stimulate X-ray emission.

(13) Yamada, S.; Kuwabara, K.; Koumoto, K. *Mater. Sci. Eng.* **1997**, *49*, 89–94.

(14) Amos, L. J.; Schmidt, M. H.; Sinha, S.; Bocarsly, A. B. *Langmuir* **1986**, *2*, 559–561.

(15) Amos, L. J.; Duggal, A.; Mirsky, E. J.; Ragonesi, P.; Bocarsly, A. B.; Bocarsly, P. A. F. *Anal. Chem.* **1988**, *60*, 245–249.

(16) Humphrey, B. D.; Sinha, S.; Bocarsley, A. B. *J. Phys. Chem.* **1984**, *88*, 736–743.

(17) Schneemeyer, L. F.; Spengler, S. E.; Murphy, D. W. *Inorg. Chem.* **1985**, *24*, 3044–3046.

(18) Kelly, M. T.; Arbuckle-Keil, G. A.; Johnson, L. A.; Su, E. Y.; Amos, L. J.; Chun, J. K. M.; Bocarsly, A. B. *J. Electroanal. Chem.* **2001**, *500*, 311–321.

(19) Wu, Y.; Pfennig, B. W.; Bocarsly, A. B.; Vicenzi, E. P. *Inorg. Chem.* **1995**, *34*, 4262–4267.

(20) Humphrey, B. D.; Sinha, S.; Bocarsley, A. B. *J. Phys. Chem.* **1987**, *91*, 586–593.

(21) Buser, H. J.; Schwarzenbach, D.; Petter, W.; Ludi, A. *Inorg. Chem.* **1977**, *16*, 2704–2709.

(22) Ludi, A.; Gudel, H. U. *Struct. Bonding (Berlin)* **1973**, *14*, 1–21.

(23) Steen, W. A.; Jeerage, K. M.; Schwartz, D. T. *Appl. Spectrosc.* **2002**, *56*.

(24) Yu, Q.; Steen, W. A.; Jeerage, K. M.; Jiang, S.; Schwartz, D. T. *J. Electrochem. Soc.* **2002**, *149*, E195–E203.

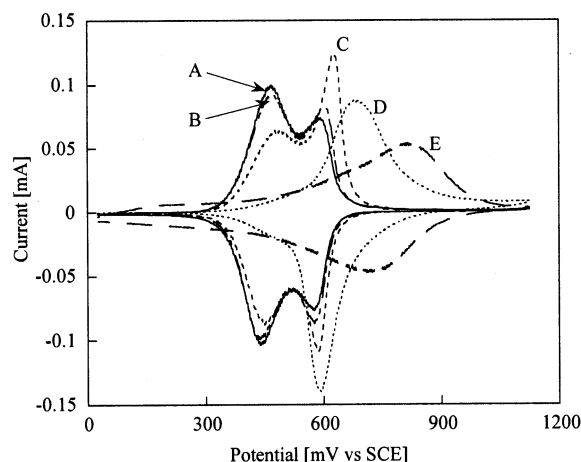


**Figure 2.** Steady-state cyclic voltammograms of five NiHCF thin films cycled in 1 M  $\text{KNO}_3$  (A), 1 M  $\text{CsNO}_3$  (E), and 1 M nitrate solutions containing  $10^{-4}$  M  $\text{CsNO}_3$  (B),  $10^{-3}$  M  $\text{CsNO}_3$  (C), and 0.5 M  $\text{CsNO}_3$  (D) with the balance  $\text{KNO}_3$ . Scan rate was 25 mV/s; only the 50th CV is shown.

Characteristic X-rays with energies between 0 and 10 keV were collected using a Si (Li) detector with a Be window (Link Systems). This permitted identification of elements with  $Z > 10$ . Each spectrum was acquired for 10 min over a  $1000 \times 1000 \mu\text{m}$  region. After background subtraction via a locally weighted least-squares error method, the peaks were fit to a Gaussian function. Thin film EDS analysis (appropriate for electrodeposited NiHCF) can be used to quantify the moles of intercalated cation in the film (see details in Jeerage et al.<sup>9,10</sup>).

**Extended X-ray Absorption Fine Structure (EXAFS).** EXAFS data were acquired on two samples cycled in 1 M  $\text{CsNO}_3$ , one reduced and one oxidized, as well as two samples cycled in 1 M  $\text{KNO}_3$ , also one reduced and one oxidized. Fe K-edge and Ni K-edge EXAFS data were acquired using PNC-CAT's insertion device beamline (Sector 20 at APS). Experiments were performed at room temperature. Samples were again spun to average the response as well as to eliminate the diffraction background from the Pt substrate. Samples were placed at a  $45^\circ$  angle to the incident X-ray beam. EXAFS data were acquired using a wide-aperture fluorescence chamber, which was placed  $90^\circ$  from the incident X-ray beam. A Z-1 filter was placed between the sample and the detector (i.e., Mn for Fe and Co for Ni). The monochromator was again detuned to  $\sim 75\%$  maximum intensity. The monochromator was calibrated using Fe and Ni foils and the absolute energy list of Kraft et al.<sup>25</sup>

Six replicate experiments were performed for each sample at the Fe K-edge, and four replicates were performed for each sample at the Ni K-edge. In the EXAFS scan range, a step size of 0.05 K was employed and an integration time of 3 s per point for the Fe K-edge and 2 s per point for the Ni K-edge. All data analysis was performed using the UWXAFS software package.<sup>26</sup> Included in this package are FEFF7, which simulates EXAFS scattering paths, and feffit2.32, which was used for performing necessary Fourier transforms.

## Results and Discussion

**General Intercalation Behavior.** Figure 2 shows cyclic voltammograms (CVs) for five separate NiHCF films cycled in pure  $\text{K}^+$  (film A), pure  $\text{Cs}^+$  (film E), and mixed  $\text{Cs}^+/\text{K}^+$  containing electrolytes (films B–D). These CVs have been capacity scaled; i.e., each CV was normalized by the total integrated area under its respective curves in order to put the CVs on the same scale. Only the 50th CV from cycling is shown. Note the two voltammetric peaks present when NiHCF is cycled in pure 1 M  $\text{KNO}_3$ ; these

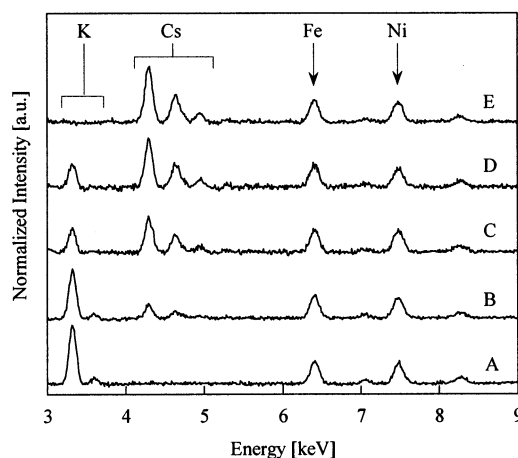


**Figure 3.** Reduced state EDS spectra of same NiHCF films shown in Figure 2. The peak at 3.3 keV is from K, the peak at 4.3 keV is from Cs, the peak at 6.4 keV is from Fe, and the peak at 7.5 keV is from Ni.

distinct peaks have been attributed to the existence of different phases within the NiHCF film.<sup>8</sup> As the concentration of  $\text{Cs}^+$  in solution is increased, the two voltammetric peaks shift toward higher potentials; eventually, only one peak is seen for the film cycled in pure 1 M  $\text{CsNO}_3$ .

NiHCF's  $\text{Cs}^+$  selectivity is apparent when probing the cation content within the matrix. Figure 3 shows Fe-normalized EDS spectra of these same films, all in the reduced state. The peaks for  $\text{K}^+$  (3.3 keV), Fe (6.4 keV), and Ni (7.5 keV) are the only features seen in the spectra for film A, as expected. (Note: the peaks from the Pt substrate are outside the range of Figure 3, and neither carbon nor nitrogen can be identified with our detector.) Even though the solution concentration of  $\text{Cs}^+$  is ca. 10 000 times less than  $\text{K}^+$  for film B, a substantial amount of  $\text{Cs}^+$  is present within the matrix, as evidenced by the size of the  $\text{Cs}^+$  peak (4.3 keV). In fact, the fractional  $\text{Cs}^+$  content (moles of  $\text{Cs}^+$ /total moles of intercalated cation) is 0.21 for film B (method to calculate intercalated  $\text{Cs}^+$  fraction described elsewhere<sup>9</sup>). Similarly, the fractional  $\text{Cs}^+$  content is 0.59 for film C, even though ca. 1000 times more  $\text{K}^+$  is present in solution than  $\text{Cs}^+$ . One might anticipate that little or no  $\text{K}^+$  should be present in the NiHCF matrix cycled in a solution containing 0.5 M  $\text{CsNO}_3$ /0.5 M  $\text{KNO}_3$  (film D). The spectrum shows that this is not the case, as the  $\text{Cs}^+$  content only increases to 0.67. Thermodynamic modeling of these selectivity trends show that strong  $\text{Cs}^+ - \text{Cs}^+$  repulsion within the matrix causes a decline in selectivity as the fractional  $\text{Cs}^+$  content becomes appreciable.<sup>27</sup> Only when the NiHCF film is exposed to a solution containing pure  $\text{Cs}^+$  does the film intercalate exclusively  $\text{Cs}^+$  cations upon electrochemically reduction (film E).

**X-ray Diffraction.** X-ray diffraction (XRD) patterns were acquired for films A–E (Figure 4). The sharp, well-defined peaks seen in Figure 4 show that these films are crystalline. Curves A and E correspond quite well to those found by Kelly et al. under similar solution conditions but using anodically derivatized films.<sup>18</sup> Kelly et al. used the [400] peak to calculate lattice parameters for anodic films intercalated with various alkali cations and found that the lattice parameter increased in proportion to cation size, going from 10.17 to 10.20 Å, for  $\text{K}^+$  and  $\text{Cs}^+$ , respectively. These cathodically deposited films have the same trend, with the lattice parameter increasing from

(25) Kraft, S.; Stumpel, J.; Becker, P.; Kuetgens, U. *Rev. Sci. Instrum.* **1996**, 67, 681–687.

(26) Stern, E. A.; Newville, M.; Ravel, B.; Yacoby, Y.; Haskel, D. *Physica B* **1995**, 209, 117–120.

(27) Jeerage, K. M.; Steen, W. A.; Schwartz, D. T. *Langmuir* **2002**, 18, 3620–3625.

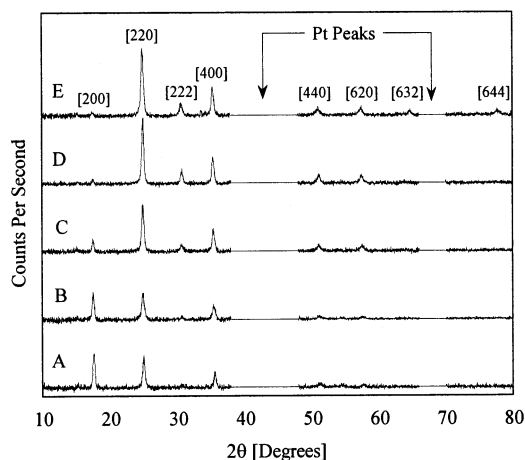


**Figure 4.** Reduced state XRD data of same NiHCF films shown in Figures 2 and 3. Diffraction peaks from the NiHCF film that were masked by the Pt substrate peaks are noted.

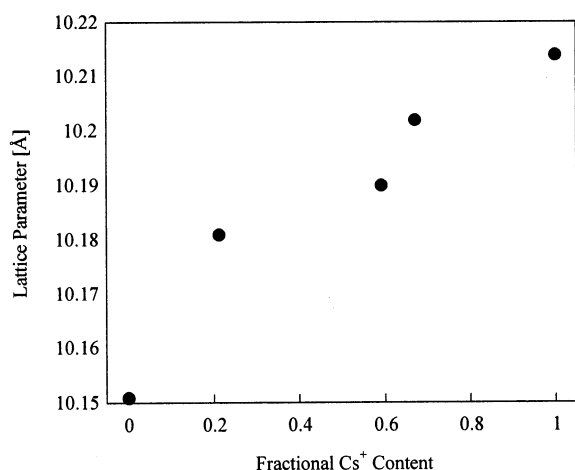


**Figure 5.** Lattice parameter as calculated from the [400] peak vs fractional Cs<sup>+</sup> content in the NiHCF film, as found using EDS spectroscopy, for the same five films shown in Figures 2–4.

10.15 to 10.21 Å for films loaded with K<sup>+</sup> and Cs<sup>+</sup>, respectively. Figure 5 is a plot of these values vs fractional Cs<sup>+</sup> content in the matrix. (Also included in Figure 5 are the films intercalated with Cs<sup>+</sup>/K<sup>+</sup> mixtures; the cation content was found using EDS.) A monotonic increase in lattice parameter is observed as the Cs<sup>+</sup> mole fraction in the matrix increases. Kelly et al. hypothesized the existence of phase segregated alkali cation microdomains in matrices possessing mixtures of different cations but did not take diffraction patterns of mixed matrices.<sup>18</sup> At the resolution of our diffraction data, we do not find a statistically significant difference between fitting the [400] peak as a homogeneous or phase-segregated material, nor is it likely that higher resolution data would help since the peak shift is small ( $\sim 0.2^\circ$ ) compared to its full width at half-maximum breadth ( $\sim 0.5^\circ$ ).

Simulations of powder XRD were also performed in an attempt to determine the exact structure of cathodically deposited NiHCF using the XRD data. Simulations for the following space groups were performed: *F*-43*m*, the “soluble” Prussian Blue analogue (Figure 1b); *Pm*-3*m*, the “insoluble” analogue with a single cation in the center of the unit cell (Figure 1a); *P*121, the “soluble” analogue with  $1\frac{1}{3}$  interstitial nicks per unit cell; and *Pmmm*, a highly Fe(CN)<sub>6</sub>-deficient material ( $\frac{4}{3}$  Fe(CN)<sub>6</sub> vacancies removed from the “soluble” analogue’s unit cell). These simulations are shown along with XRD data taken of oxidized films

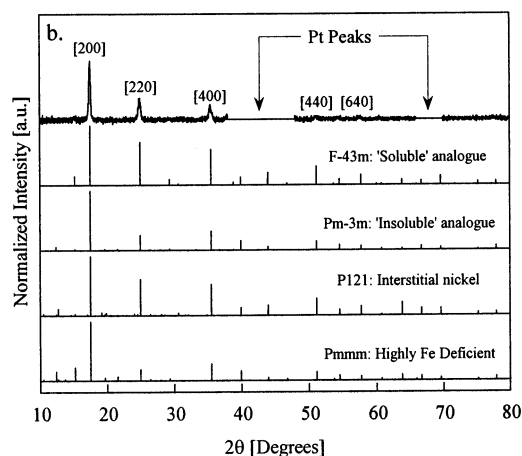
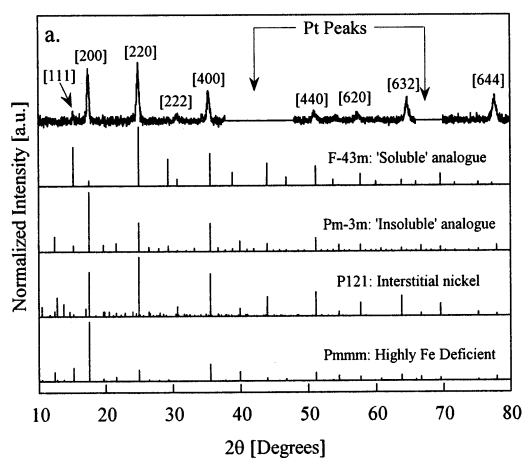


**Figure 6.** XRD pattern for Cs<sup>+</sup> (Figure 6a) and K<sup>+</sup> (Figure 6b) intercalated, oxidized NiHCF thin films. Also shown are simulation patterns for several different possible structures.

intercalated with Cs<sup>+</sup> (Figure 6a) and K<sup>+</sup> (Figure 6b). (Note: simulations of reduced films show similar results; only oxidized simulations are included for brevity.) The simulations do not include intercalated water molecules, weak X-ray scatters known to be incorporated in the matrices.<sup>28</sup> Nonetheless, the simulations in Figure 6a,b compare well with those which do include intercalated water.<sup>13</sup>

Comparison of the simulations and the actual data shows that virtually every reflection seen in the actual data is also seen in all the simulations. Because this class of compounds retains its cubic structure over a wide range of stoichiometries, the low index peaks are conserved.<sup>21,22</sup> This leaves analysis of relative peak intensities as the means for refining the structure, which cannot be done reliably when comparing a textured thin film to a powder pattern. Thus, Figures 4–6 confirm that cathodically deposited NiHCF is a crystalline solid falling within the typical space groups found for bulk NiHCF powders. But, we are unable to provide a more refined structure without using an alternative approach.

**Extended X-ray Absorption Fine Structure (EXAFS).** Given that XRD shows the film is crystalline with a cubic structure, the Ni and Fe coordination environment can provide definitive evidence to further refine the structure. Each of the space groups simulated in Figure 6 has quite distinctive local coordination environments. All have Fe octahedrally coordinated to C≡N (Fe coor-

(28) Lasky, S. J.; Buttry, D. A. *J. Am. Chem. Soc.* **1988**, *110*, 6258–6260.

dination =  $N_{\text{Fe}} = 6$ ), but the nickel environment changes. The *F*-43*m* group has Ni 100% octahedrally coordinated to N≡C ( $N_{\text{Ni}}$  coordination =  $N_{\text{Ni}} = 6$ ). The *Pm*-3*m* group has Ni as 75% square-planar and 25% octahedrally coordinated to N≡C, resulting in  $N_{\text{Ni}} = 4.5$ . The *P*121 space group has Ni as 75% octahedrally coordinated to N≡C and 25% uncoordinated ( $N_{\text{Ni}} = 4.5$ ), while the *Pmmm* group has  $N_{\text{Ni}} = 4$ . Not only does the coordination number vary, but also the local order. For example, the *Pm*-3*m* and *P*121 groups both have  $N_{\text{Ni}} = 4.5$ , but in the *Pm*-3*m* group all the nickel atoms are locked into the matrix whereas the *P*121 group has mobile, interstitial nickel. In short, this material possesses ideal traits for EXAFS, a technique which has been used in the past to study the structure of electrochemical materials (see refs 29–31 for some typical results).

EXAFS data and analysis have been presented for bulk NiHCF materials<sup>32</sup> as well as other Prussian Blue analogues.<sup>33–36</sup> Fe K-edge EXAFS data had been presented for anodic NiHCF thin films, but the lack of Ni K-edge data precluded a definitive structural assessment.<sup>37</sup> Representative X-ray fluorescence data normalized by the incident X-ray intensity ( $I_{\text{F}}/I_{\text{O}}$ ) is plotted vs energy for a  $\text{K}^+$  loaded, reduced, NiHCF thin film in Figures 7a (Fe K-edge) and 7b (Ni K-edge). The preedge feature in Figure 7b is not due to  $I_{\text{O}}$ , and thus must be attributed to  $I_{\text{F}}$ , though its origin remains unknown. Because of this preedge feature and the highly delocalized charges characteristic of this system,<sup>24</sup> we have not analyzed the edge or near-edge data but instead focus on the EXAFS region.

For the actual analysis, EXAFS data ( $\chi(k)$ ) were extracted from  $I_{\text{F}}/I_{\text{O}}$  by first subtracting the atomic background from the raw data. The background was extrapolated to the absorption edge, a procedure typical for this type of analysis. This means that the dip seen in Figure 7b was effectively ignored. A  $k$  range of ca. 3–8 Å<sup>−1</sup> was then used for further analysis. (Specific ranges are shown in Table 1.) The refined structure of NiHCF is governed by variations in the nickel atoms local environment; these variations are determined by fitting structural models to the Fourier transformed EXAFS data. Thus,  $k^2\chi(k)$  data were Fourier transformed into  $r$ -space (distance in angstroms), and simulated EXAFS for various structural models were created in FEFF7.

Before fitting a structural model to the data, we must understand what happens when the nickel coordination is less than 6. For solution precipitated bulk metal hexacyanoferrates, oxygen atoms (from intercalated

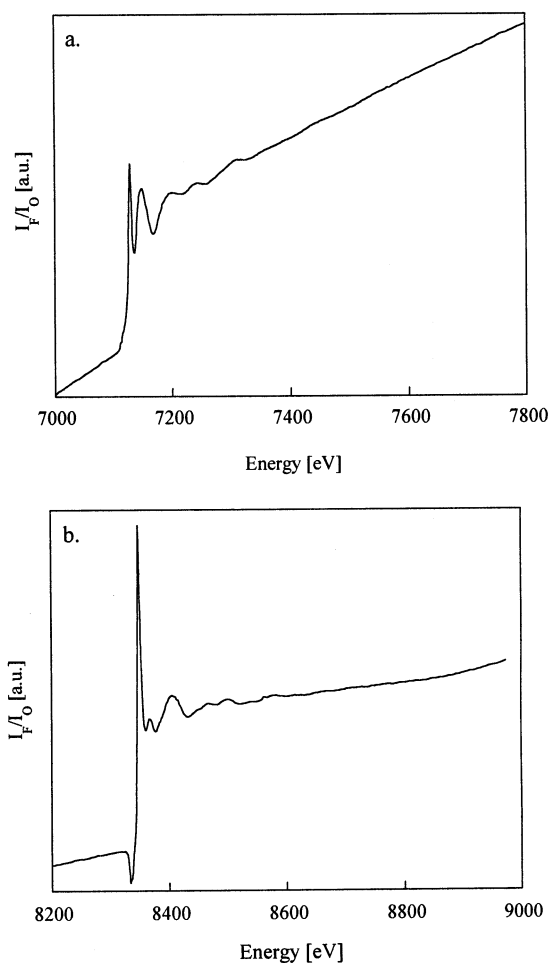


**Figure 7.** Fe K-edge (a) and Ni K-edge (b) data for a NiHCF film loaded with  $\text{K}^+$  ions in the reduced state.

water) are known to complete nickel's coordination sphere.<sup>13,33,34,38</sup> Some groups analyzing EXAFS data of these compounds simply treat the oxygen as if it were nitrogen<sup>34</sup> while others rationalize that its contribution is negligible and ignore it altogether.<sup>33</sup> Here, we largely avoid this issue by determining values for the nickel atom's coordination ( $N_{\text{Ni}}$ ) using the second and third spheres, comprised of carbon and Fe. For the first coordination sphere we use the approach of Yokoyama et al.<sup>34</sup>

To eliminate the strong correlation between the product  $N_{\text{Ni}}S_0^2$  ( $S_0^2$  is the constant amplitude factor) and  $\sigma^2$  (Debye–Waller factor), which prohibits an independent determination of  $N_{\text{Ni}}S_0^2$ , a simultaneous fit of the nickel and iron edges was performed. Simultaneously fitting two relevant edges not only breaks the correlation between  $N_{\text{Ni}}S_0^2$  and  $\sigma^2$ , it also forces physically significant variables (e.g., the distance between Fe and Ni atoms) to be the same. What remains is to separate  $N_{\text{Ni}}$  from  $S_0^2$ . Measurements of known structures with known coordination values have determined  $S_0^2$  to be 0.90 ( $\pm 5\%$ ) for copper when using the UWXAFS software package for analysis.<sup>39</sup> Because  $S_0^2$  is insensitive to changes in local chemical environment and since it is expected to be similar for all transition metals,<sup>40</sup> 0.90 can be used with confidence here.

(29) Balasubramanian, M.; Sun, X.; Yang, X. Q.; McBreen, J. *J. Power Sources* **2001**, 92, 1–8.

(30) Mo, Y. B.; Antonio, M. R.; Scherson, D. A. *J. Phys. Chem. B* **2000**, 104, 9777–9779.

(31) Totir, D.; Mo, Y. B.; Kim, S.; Antonio, M. R.; Scherson, D. A. *J. Electrochem. Soc.* **2000**, 147, 4594–4597.

(32) Hallmeier, K. H.; Sauter, S.; Szargan, R. *Inorg. Chem. Commun.* **2001**, 4, 153–156.

(33) Giorgetti, M.; Berrettoni, M.; Filipponi, A.; Kulesza, P. J.; Marassi, R. *Chem. Phys. Lett.* **1997**, 275, 108–112.

(34) Yokoyama, T.; Ohta, T.; Sato, O.; Hashimoto, K. *Phys. Rev. B* **1998**, 58, 8257–8266.

(35) Moulin, C. C. D.; Villain, F.; Bleuzen, A.; Arrio, M. A.; Saintavit, P.; Lomenech, C.; Escax, V.; Baudet, F.; Dartyge, E.; Gallet, J. J.; Verdager, M. *J. Am. Chem. Soc.* **2000**, 122, 6653–6658.

(36) Kulesza, P. J.; Malik, M. A.; Skorek, J.; Miecznikowski, K.; Zamponi, S.; Berrettoni, M.; Giorgetti, M.; Marassi, R. *J. Electrochem. Soc.* **1999**, 146, 3757–3761.

(37) Hess, N. J.; Sukamto, S.; Rassat, R. T.; Hallen, R. T.; Orth, R. J.; Lilga, M. A.; Lawrence, W. E. *Mater. Res. Soc. Symp. Proc.* **1997**, 465, 813–817.

(38) Bleuzen, A.; Lomenech, C.; Escax, V.; Villain, F.; Varret, F.; Moulin, C. C. D.; Verdager, M. *J. Am. Chem. Soc.* **2000**, 122, 6648–6652.

(39) Frenkel, A. I.; Machavariani, V. S.; Rubinstein, A.; Rosenberg, Y.; Voronel, A.; Stern, E. A. *Phys. Rev. B* **2000**, 62, 9364–9371.

(40) Stern, E. A.; Bunker, B. A.; Heald, S. M. *Phys. Rev. B* **1980**, 21, 5521–5539.

Table 1. Simulations Fe and Ni K-Edge EXAFS Fitting Results

	reduced, K <sup>+</sup> loaded	oxidized, K <sup>+</sup> loaded	reduced, Cs <sup>+</sup> loaded	oxidized, Cs <sup>+</sup> loaded
$R_{\text{Ni-N}}$ [Å]	2.06 ± 0.01	2.07 ± 0.01	2.07 ± 0.02	2.07 ± 0.02
$R_{\text{Ni-C}}$ [Å]	3.24 ± 0.00	3.25 ± 0.01	3.25 ± 0.00	3.25 ± 0.00
$R_{\text{Ni-Fe}}$ [Å]	5.14 ± 0.01	5.16 ± 0.02	5.17 ± 0.02	5.17 ± 0.02
$\Delta E_{0,\text{Ni-N}}$ [eV]	-0.84 ± 1.42	-1.24 ± 1.52	-0.78 ± 1.85	-0.76 ± 1.64
$\Delta E_{0,\text{Ni-C}}$ [eV]	3.12 ± 1.53	3.53 ± 1.69	3.24 ± 1.84	3.64 ± 1.69
$\Delta E_{0,\text{Ni-Fe}}$ [eV]	5.00 ± 1.73	5.13 ± 1.81	4.85 ± 2.04	5.16 ± 1.83
$\Delta E_{0,\text{Fe-C}}$ [eV]	-2.05 ± 0.47	-1.40 ± 0.66	-1.98 ± 0.44	-1.09 ± 0.46
$\Delta E_{0,\text{Fe-N}}$ [eV]	0.05 ± 0.99	0.70 ± 1.30	1.28 ± 0.88	0.41 ± 0.97
$\Delta E_{0,\text{Fe-No}}$ [eV]	4.71 ± 1.96	2.89 ± 1.92	2.42 ± 1.78	2.68 ± 1.61
$\sigma^2_{(\text{Ni-N})}$ [Å <sup>2</sup> ]	0.002 ± 0.001	0.002 ± 0.001	0.006 ± 0.002	0.003 ± 0.001
$\sigma^2_{(\text{Ni-C})}$ [Å <sup>2</sup> ]	0.003 ± 0.001	0.002 ± 0.005	0.002 ± 0.006	0.003 ± 0.001
$\sigma^2_{(\text{Ni-Fe})}$ [Å <sup>2</sup> ]	0.011 ± 0.003	0.011 ± 0.003	0.011 ± 0.002	0.011 ± 0.002
$\sigma^2_{(\text{Fe-C})}$ [Å <sup>2</sup> ]	0.003 ± 0.001	0.004 ± 0.001	0.005 ± 0.001	0.003 ± 0.001
$\sigma^2_{(\text{Fe-N})}$ [Å <sup>2</sup> ]	0.002 ± 0.001	0.003 ± 0.001	0.003 ± 0.001	0.003 ± 0.001
$N_{\text{Ni}}$	4.4 ± 1.3	5.1 ± 2.6	5.1 ± 2.8	4.7 ± 1.5
$N_{\text{Fe}}$	6.0	6.0	6.0	6.0
$N_{\text{IndP}}$	28	28	28	28
$N_{\text{vars}}$	15	15	15	15
DOF	13	13	13	13
$\chi^2_{\nu}$	48	69	95	70
$r$ -factor, Ni K-edge <sup>a</sup>	3%	3%	4%	3%
$r$ -factor, Fe K-edge <sup>b</sup>	1%	1%	1%	1%

<sup>a</sup> Ni edge EXAFS used data between 2.7 and 8 Å<sup>-1</sup>. <sup>b</sup> Fe edge EXAFS used data between 2.95 and 8 Å<sup>-1</sup>.

Multiple scattering paths predicted by FEFF7 were included in structural models because of the strong focusing effect of the linear Fe-C≡N-Ni chains; only linear scattering paths were included (i.e., weaker triangular paths were ignored). Finally, no contribution from interstitial alkali cations were included; their contribution to the EXAFS is negligible compared to that of the Fe-C≡N-Ni chains.

Figure 8a,b contains plots of Fe K-edge EXAFS for K<sup>+</sup> and Cs<sup>+</sup> intercalated, oxidized and reduced, NiHCF thin films. Figure 8a is reduced EXAFS,  $k^2\chi(k)$ , vs wavenumber. Only the range of data used for further analysis is shown (i.e., ~3–8 Å<sup>-1</sup>). Although the fit was actually done in  $r$ -space (Figure 8b), both the actual data and the fit are shown in Figure 8a. The Fourier transformed  $k^2\chi(k)$  data are graphed vs pseudo-radial distance ( $R_{\text{pseudo}}$ , which is not corrected for phase shifts) in Figure 8b. The first peak in Figure 8b is due to interactions with carbon atoms ( $R_{\text{pseudo}} \approx 1.3$  Å), the second is due to nitrogen atoms ( $R_{\text{pseudo}} \approx 2.5$  Å), and the third is a result of Ni ( $R_{\text{pseudo}} \approx 4.5$  Å). The quality of the data is such that no peaks are distinguishable beyond  $R_{\text{pseudo}} \approx 5.5$  Å. The model was fit to the data between the vertical lines (0.95 Å <  $R_{\text{pseudo}}$  < 5.5 Å). The fit is excellent; with an  $r$ -factor of around 1% (2% or less is generally regarded as an excellent fit, with values slightly greater being acceptable). Values for the  $r$ -factor are reported in Table 1.

Also reported in Table 1 are the number of independent points ( $N_{\text{IndP}} = 28$ ) for the simultaneous fit;  $N_{\text{IndP}}$  is determined from the  $k$  and  $r$  ranges used. Since only 15 variables ( $N_{\text{vars}}$ ) were needed, 13 degrees of freedom (DOF) remain. The value for  $\sigma^2_{(\text{Fe-Ni})}$  is ca. 0.012 Å<sup>2</sup>, which is greater than one might expect on the basis of the values of  $\sigma^2$  for the Ni-N, Ni-C, Fe-C, and Fe-N interactions (each ca. 0.003 Å<sup>2</sup>) and the fact that the linear Fe-C≡N-Ni chain is tightly bound. On the basis of these values of  $\sigma^2_{(\text{Fe-Ni})}$ , one can assume that the Fe and Ni atoms oscillate symmetrically to one another; this implies that the Fe-C≡N-Ni chain's center of mass remains relatively fixed. The value of  $\chi^2_{\nu}$  (reduced  $\chi^2$ , a measurement of error roughly calculated by summing the squared differences between data and fit and dividing that value by the DOF) is also shown in Table 1.  $\chi^2_{\nu}$  equals one if errors are due entirely random noise, but since  $\chi^2_{\nu}$  is greater than one, the fit is dominated by systematic errors. Uncertainties

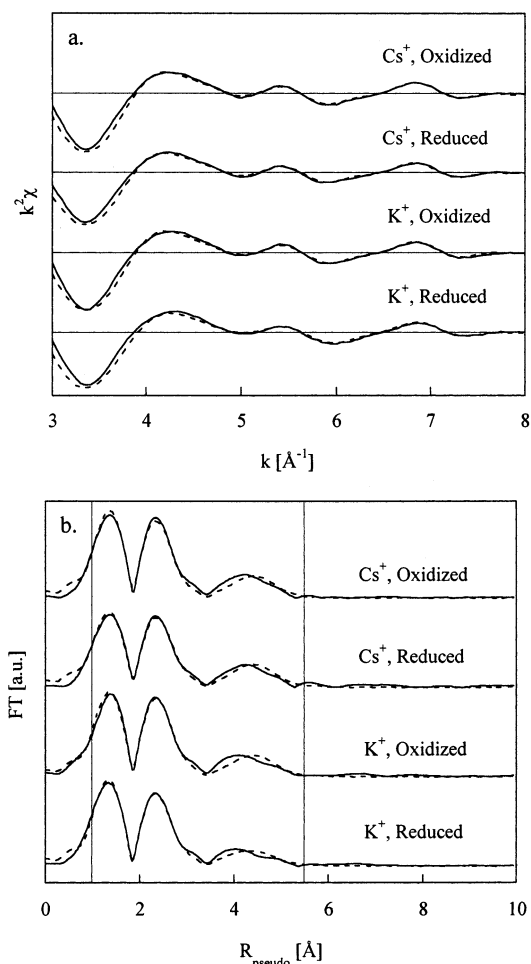


**Figure 8.** Fe K-edge data and fits for four NiHCF films loaded with K<sup>+</sup> and Cs<sup>+</sup> in both the reduced and oxidized states. (a) is  $k^2\chi(k)$  vs Å<sup>-1</sup> while (b) is Fourier transformed data in  $r$ -space (Å). Fitting was between the vertical lines in (b) (0.95 Å <  $R_{\text{pseudo}}$  < 5.5 Å) and was done simultaneously with Ni K-edge. Important parameters are reported in Table 1. Actual data is shown as — while the fit is shown as - - - in both (a) and (b).

in individual variables must be multiplied by  $\chi^2_{\nu}$  to account for these systematic errors; this was done, and the uncertainties shown in Table 1 reflect this.<sup>26</sup> The high

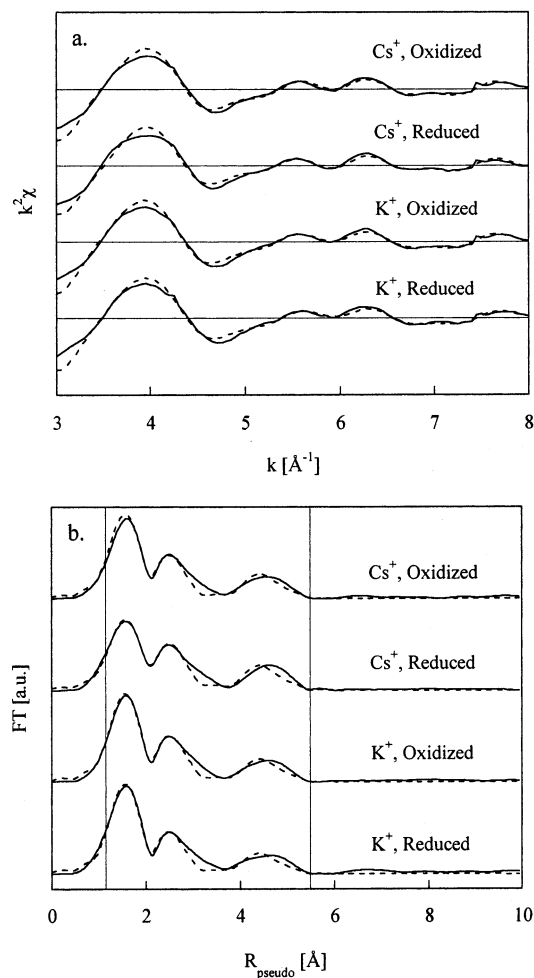


**Figure 9.** Ni K-edge data and fits for the same four NiHCF films shown in Figure 8. Fitting was done between the vertical lines in (b) ( $R_{\text{pseudo}} = 1.2$  and  $5.5$  Å) and is shown as --- while actual data are shown as —. Fitting of Ni K-edge and Fe K-edge was done simultaneously. Important parameters are reported in Table 1.

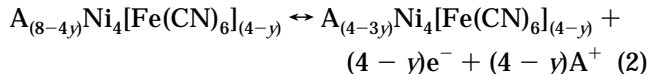
degree of accuracy (low  $r$ -factors) seen in Figure 8a,b and Table 1 give us confidence that the Fe coordination is indeed 6, and since  $\sigma^2_{(\text{Fe-Ni})}$  has been found,  $N_{\text{Ni}}$  can be independently determined.

Parts a and b of Figure 9 are Ni K-edge plots analogous to those in parts a and b of Figure 8. The peaks in Figure 9b are from nitrogen, carbon, and Fe atoms ( $R_{\text{pseudo}} \approx 1.5$ ,  $2.5$ , and  $4.5$  Å, respectively). The fit is good ( $r$ -factor values around 3%), although not as precise as the Fe-edge. Lattice parameters were estimated from the EXAFS based on the assumption that all distances are collinear; these lattice parameters are systematically about  $0.1$  Å larger than the values found using XRD. When distances calculated from local data (EXAFS) are larger than distances calculated from periodic data (XRD), local disorder exists.<sup>41–44</sup> Defects within the structure cause the supposedly linear Fe—C≡N—Ni chain to deviate from collinearity, an event known as angular buckling. Thus, adding the interatomic distances between Fe—C, C≡N,

and N—Ni would be greater than the distance directly between Fe—Ni. The observed difference in lattice parameter is indicative of a less rigid structure and Fe(CN)<sub>6</sub> vacancies. This type of behavior has been observed in other systems.<sup>41–44</sup> Finally, the mean nickel coordination numbers determined for the various films tested fall between 4.4 and 5.1. (Exact values with their uncertainties are given in Table 1.)

These structural findings have strong implications for the stoichiometry and reversible ion intercalation behavior of this material. As noted above, both the  $Pm\text{-}3m$  and  $P121$  space groups have an average nickel coordination number of 4.5. Despite this, the data here are more consistent with the  $Pm\text{-}3m$  space group.  $N_{\text{Ni}}$  values less than 6 could not result simply from the presence of the interstitial nickel atoms seen in group  $P121$ . The quantity measured and reported as  $N_{\text{Ni}}$  is the coordination of nickel atoms locked in the matrix; all nickel locked in the matrix in space group  $P121$  are still 6-fold coordinated. If present, interstitial nickel atoms would generate additional EXAFS peaks unique to its environment and in areas not associated with the Ni—C and Ni—Fe interactions used to calculate  $N_{\text{Ni}}$ . The 1% greater lattice parameters found using EXAFS compared to XRD also support Fe(CN)<sub>6</sub> vacancies.

Taken together, these results provide a consistent picture where the average structure for cathodically deposited NiHCF resembles Figure 1a and the reaction stoichiometry is close to eq 1. In Prussian Blue analogues, one normally describes the solid in terms of Fe(CN)<sub>6</sub> vacancies rather than nickel coordination. With this in mind, we can rewrite the NiHCF redox reaction in a general form as



Here,  $y$  denotes the average number of Fe(CN)<sub>6</sub> vacancies per unit cell. From eq 2, we see that  $N_{\text{Ni}} = 6 - 1.5y$ . Combining this relationship with the values for  $4.4 < N_{\text{Ni}} < 5.1$ , we predict  $0.6 < y < 1.1$ . In completely independent experiments published elsewhere, we have made measurements of the intercalated cation content in the oxidized and reduced matrix and also determined  $y \approx 1$ .<sup>10</sup>

## Conclusions

XRD and EXAFS data of cathodically deposited NiHCF thin films generally support a structure analogous to “insoluble” Prussian Blue (Figure 1a). Our textured films prohibit making conclusive structural determinations based on XRD alone, but the XRD data do confirm a cubic structure. The lattice parameter is seen to monotonically increase with increasing Cs<sup>+</sup> content in the matrix. Lattice parameters found using EXAFS data are generally  $0.1$  Å greater than those found from XRD. This trend is indicative of local disorder or angular buckling. For our system, local disorder means randomly located Fe(CN)<sub>6</sub> vacancies. Values for the average nickel coordination obtained by simultaneously fitting Fe and Ni K-edge EXAFS data are between 4.4 and 5.1. These nickel coordination values, and the EXAFS results in general, are consistent with Ni:Fe ratios found independently for cathodically deposited NiHCF. These results also support a more open, more Fe(CN)<sub>6</sub>-deficient material than “soluble” Prussian Blue, the material normally assumed as the electroactive form of NiHCF. The data were inconsistent with appreciable amounts of interstitial nickel. These results show that the relationship between

(41) Frenkel, A.; Stern, E. A.; Voronel, A.; Qian, M.; Newville, M. *Phys. Rev. Lett.* **1993**, *71*, 3485–3488.

(42) Frenkel, A.; Stern, E. A.; Voronel, A.; Qian, M.; Newville, M. *Phys. Rev. B* **1994**, *49*, 11662–11674.

(43) Frenkel, A.; Voronel, A.; Katzir, A.; Newville, M.; Stern, E. A. *Physica B* **1995**, *209*, 334–336.

(44) Frenkel, A. I.; Stern, E. A.; Voronel, A.; Heald, S. M. *Solid State Commun.* **1996**, *99*, 67–71.

material stoichiometry and structure seen in bulk NiHCF can also be applied to electrodeposited thin films.

**Acknowledgment.** This work was supported by the DOE Environmental Molecular Science Program (FG07-97ER14819) and the EPA/NSF Technology for a Sustainable Environment Program (CTS-9729046). PNC-CAT is supported by the U.S. Department of Energy, Basic Energy

Services, under Grant DE-FG03-97ER45629, the University of Washington, and grants from the Natural Sciences and Engineering Council of Canada. Use of the Advanced Photon Source was supported by the U.S. Department of Energy, Basic Energy Sciences, Office of Science, under Contract W-31-109-Eng-38.

LA020352E